Pacific Northwest
NATIONAL LABORATORY

PNNL-31453

A Comparative Analysis of Lithium-Ion Battery Chemistries for Cold-Climate Maritime Applications

June 2021

Nolann Williams
Dongping Lu
James McVey
Robert J. Cavagnaro

U.S. DEPARTMENT OF ENERGY

Prepared for the U.S. Department of Energy
under Contract DE-AC05-76RL01830

DISCLAIMER

PACIFIC NORTHWEST NATIONAL LABORATORY
operated by
BATTELLE
for the
UNITED STATES DEPARTMENT OF ENERGY
under Contract DE-AC05-76RL01830

Printed in the United States of America

Available to DOE and DOE contractors from the
Office of Scientific and Technical Information,
P.O. Box 62, Oak Ridge, TN 37831-0062;
ph: (865) 576-8401
fax: (865) 576-5728
email: reports@adonis.osti.gov

Available to the public from the National Technical Information Service
5301 Shawnee Rd., Alexandria, VA 22312
ph: (800) 553-NTIS (6847)
email: orders@ntis.gov <https://www.ntis.gov/about>
Online ordering: http://www.ntis.gov

PNNL-31453

A Comparative Analysis of Lithium-Ion Battery Chemistries for Cold-Climate Maritime Applications

June 2021

Nolann Williams
Dongping Lu
James McVey
Robert J. Cavagnaro

Prepared for
the U.S. Department of Energy
under Contract DE-AC05-76RL01830

Pacific Northwest National Laboratory
Richland, Washington 99354

Contents

Figures

1.0 Executive Summary

Energy storage, primarily in the form of electrochemical batteries, is critical for enabling integration of marine energy (e.g., power from waves and currents) with end-use applications at sea due to the periodicity of the resources and requirement of consistent, smooth power delivery. Powering high-latitude coastal or ocean-based observing systems has been identified as a high value-proposition use case, exemplifying the concept of Powering the Blue Economy. An existing power system implementation for such a platform uses solar panels coupled to rechargeable lithium-ion batteries, augmented by a non-rechargeable backup bank used to power heaters in winter months. As wave energy is a potential resource for powering this and similar use cases and is strongest when solar power is most limited, it was hypothesized that integration of wave power would alleviate some of the challenges in cold climates related to energy storage. In this work, we investigate the use case scenario in simulation and perform a comparative experimental campaign of commercially-available lithium-ion battery chemistry formulations to determine the most appropriate choice for the application. The experiment compared the most commonly-used lithium-based battery types (NCM, NCA, and LFP) in laboratory conditions emulating a battery enclosure thermally coupled to freezing seawater using an industrial battery performance tester in PNNL's arctic simulation lab. Battery strings were repeatedly cycled (i.e., charged, discharged, rested) and their usable capacity was measured. Both NCM and NCA strings exhibited degradation upon cycling, while the LFP string maintained stable operation through over 700 complete cycles. Though lower in baseline capacity, LFP are recommended for this and similar low-temperature applications with access to high levels of bulk charging current (e.g., from high-energy wave events) and their use may reduce the cost and complexity of battery conditioning and protection apparatus.

2.0 Introduction & Background

Ocean observing platforms distributed along coasts and throughout the oceans provide vital measurements of the sea and atmosphere. These data are critical for weather forecasting, water quality monitoring, public health and safety, and to track the changing climate. The societal value of ocean observations, high costs of energy associated with powering them, and co-location with abundant marine energy (i.e., power from waves, currents, or thermal gradients) sources resulted in inclusion as a Power at Sea market for the US DOE Powering the Blue Economy (PBE) report and portfolio of research activities (LiVecchi et al. 2019). Subsequent outreach and engagement with experts in the field identified gaps of capabilities and opportunities of what could be done with more power available. Experts signaled that extending observing system mission duration, increasing sampling rate, and enabling more sensors with more options were the highest priorities of improvements that could be realized with enhanced energy availability (Green et al. 2019). Several observing platforms of the numerous discussed by experts were chosen for deeper analysis as high value proposition use cases for integration with marine energy, representing a mix of ocean locations (e.g., at surface or subsea), distance from shore (e.g., nearshore, far offshore), and platform types (e.g., stationary and mobile) (Cavagnaro, Copping, et al. 2020). Coastal weather buoys (CWBs), specifically those operated by the National Oceanographic and Atmospheric Administration (NOAA) National Data Buoy Center (NDBC) were among the five use cases detailed (LiVecchi et al. 2019).

Through analysis of available literature, buoy specifications, and direct feedback from NDBC personnel, we learned the power requirements and approximate duty cycles for CWBs, the major components of their power generation and energy storage system, and challenges operating systems at high latitude. CWBs rely on a small array of solar panels positioned at the top of the buoy to power sensing systems and charge a battery bank. Older generations of buoys utilized lead acid batteries (Chew, Pelaccio, and Johnson 2002) likely due to their low cost and high reliability. However, the latest generation of CWB sensor and power management package, known as SCOOP, replaces the rechargeable lead acid batteries with Li-ion. Battery packs are augmented with heaters to maintain health in colder waters of the Atlantic Ocean and Great Lakes, and further augmented with lithium primary batteries to cover increased heating load in Pacific and coastal Alaskan waters north of 48° (L. LeBlanc, personal communication, May 2020). Utilizing power from waves to augment solar power was identified as an opportunity to enable improved performance (A. Copping et al. 2018). However, improvements may also be realized by selecting a Li-ion formulation more amenable to the environmental and power cycle conditions experienced by high latitude CWBs and similar ocean observing platforms.

Recent and projected trends in battery utilization show a massive increase of market share to Li-ion for rechargeable applications, primarily driven by expanded use in portable electronics and road transportation (Zubi et al. 2018). The major factors contributing to this trend are their exceptionally high energy density, stable voltage discharge characteristics, and relatively high cycle life. The shift to Li-ion batteries in ocean observing systems mirrors the general trend, as they are now predominately used in CWBs, drifting profiling oceanographic floats, and autonomous underwater vehicles (Cavagnaro, Matthews, et al. 2020). However, performance, reliability, and safety issues under use at low temperature remain (Ouyang et al. 2019). For example, safety and robustness are reported as the top two requirements for battery system design by NDBC engineers, who cite conservative over-engineering of their batteries and including additional cells as design choices for their high-latitude systems (L. LeBlanc, personal communication, May 2020).

An additional concern arises when considering coupling wave energy converter (WEC) systems to ocean observing platforms. The intermittent and highly-variable nature of the wave energy resource may result in charge and discharge characteristics for a coupled battery bank

that are distinct from solar technology currently employed by CWBs and similar platforms. The performance of a combined wave and solar-powered observing system operated in Hawaii, depicted in Fig. 1, illustrated how the average power output over a period of days may cover the full load, but low wave conditions during the period result in high rates of battery discharge followed by rapid charging when waves return, for example, from a storm (Joslin et al. 2019). Seasonality of the resource (i.e., stronger waves are more common in winter months) and conditions resulting from storms are common for WEC power profiles sited throughout the oceans; combined with Li-ion storage at low temperatures at higher latitudes, there is opportunity to evaluate the performance of this novel use case.

Figure 1. The Wave Powered Adaptable Monitoring Package aboard the Fred. Olsen Bolt. Courtesy of PMEC

The goal of this work is to determine if there are preferable battery chemistries and cell operation protocols to improve the performance and extend cycle life of Li-ion-based energy storage systems for at-sea applications in cold climates. First, we review existing relevant energy storage technology, then we consider a use case of the NDBC SCOOP platform operating above 48° N in simulation to determine implications of coupling wave energy harvesting to a representation of the buoy power system at a location of interest. We follow by conducting laboratory battery performance characterization in emulated conditions of freezing seawater, comparing strings of three commercially-available Li-ion battery chemistries. We present results from these studies, and conclude with recommendations for battery selection and future research pathways.

2.1 Overview of battery energy storage technologies for PBE applications

For effective delivery of marine energy to offshore applications, rechargeable batteries are considered a necessary energy storage technology. Batteries are required to buffer through the natural periodicity of both wave and tidal energy resource profiles and deliver smooth power to electrical loads. Rechargeable batteries employ highly reversible reactions, leading to extended service life, high reliability, and limited maintenance. Various rechargeable battery technologies have been developed and deployed for different applications. Here, we review the major technologies, with a focus on those potentially suitable for the use case of marine energy in cold climates.

2.1.1 Lead-acid batteries

The lead-Acid battery (Fig. 2a) is one of the oldest and most widespread rechargeable batteries. Valve regulated lead acid (VRLA) is pervasive for diverse applications including most cars because of high technology maturity, low cost, and high reliability (Parker 2001). Moreover, it doesn't need special maintenance and the self-discharge rate is very low – only 2-5% per month, which makes it possible for long-term energy storage. Lead-Acid battery technology usually has a service life of 800 to 1800 cycles or 5-15 years of operation, which depends on the depth of discharge (DOD) and working temperature. For example, long term use at full discharge may influence electrode stability, decreasing the service life. In addition, temperature plays an important role on cell performance and lifespan: relatively higher temperature (>45 °C) helps to improve rate capability but reduces cell life, while low temperatures (<-5°C) will lower cell efficiency and similarly reduce cell life. One drawback of the technology is low system specific energy (30 Wh/kg) and power density (150 W/kg) (Hadjipaschalis, Poullikkas, and Efthimiou 2009). So called 'marine' lead acid batteries are often of the absorbent glass mat (AGM) variety as they require no maintenance and are tolerant of large amplitude motion (no liquid-state chemicals). Lead acid batteries are available worldwide and are easy to ship.

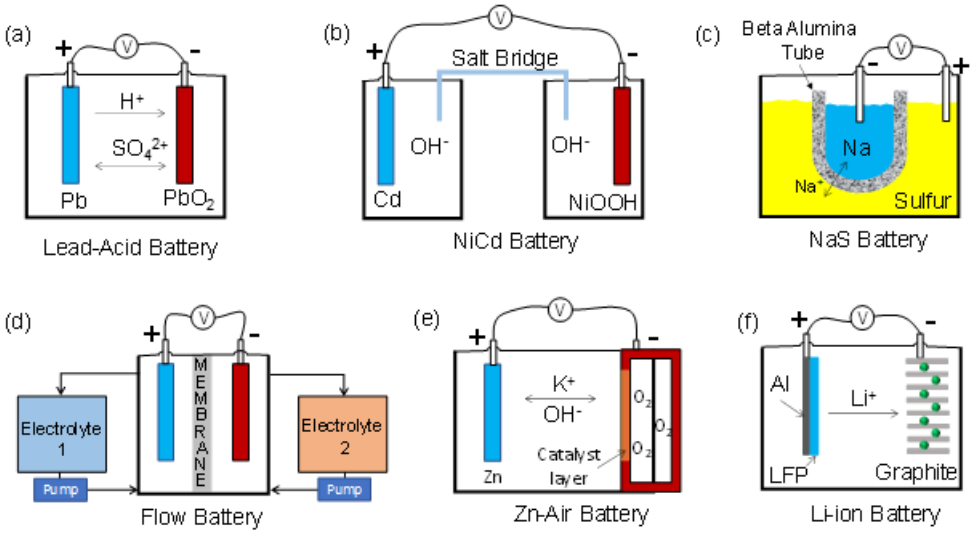

Figure 2. Schematic of six kinds of rechargeable battery systems. a) Lead-Acid battery; b) NiCd battery; c) NaS battery; d) Flow battery; e) Zn-air battery; f) Li-ion battery

2.1.2 Nickel-based batteries

The nickel-cadmium (NiCd) battery is the first generation of Nickel-based batteries (Fig. 2b), which was a preferred power source for two-way radios, professional video cameras and power tools, owing to its long cycle life (about 3000 cycles), deep discharge characteristic and fast recharging ability (Divya and Østergaard 2009). Due to the environmental concerns surrounding the use of cadmium, this formulation was largely replaced by the nickel-metal-hydride (NiMH) battery. However, this battery has a shortened cycle life if repeatedly used at high load currents and suffers from a memory effect (reduced capacity after repeated shallow charge and discharge) (Zhou et al. 2012). The nickel-zinc (NiZn) battery is another type of Ni-based battery, which has excellent deep discharge capability without using heavy toxic materials. However,

NiZn batteries suffer from high self-discharge and short cycle life caused by Zn dendrite growth. The specific energies of the NiCd, NiMH and NiZn are 50 Wh/kg, 80 Wh/kg and 60 Wh/kg, respectively, superior to lead-acid cells (Zhou et al. 2012).

2.1.3 Molten salt batteries

Molten salt based batteries like the Sodium Sulphur (NaS) battery (Fig. 2c) and Sodium Nickel Chloride ($NaNiCl_2$) battery have high potential for large scale energy storage. NaS batteries consist of liquid sodium (anode) and liquid sulfur (cathode), separated by a solid beta alumina ceramic electrolyte (Sudworth 1984). The high operating temperature (300-500°C) and strong causticity of the sodium polysulfides used limit its suitability to stationary (i.e., immobile) energy storage. High energy density (100 Wh/kg), long cycle life (2500 full discharge cycles), high energy efficiency (around 89%) and cheap and recyclable raw materials make the NaS battery a potential cell for commercial electrical energy storage, such as grid support, wind power integration and high-value grid services. Additional drawbacks of the technology are high capital cost and high flammability when in contact with air and moisture, limiting their potential for use at sea.

A second kind of molten-salt battery, NaNiCl2, is operated at the lower end of the molten-salt battery temperature range, compared with NaS (G. Li et al. 2016). $NaNiCl_2$ cells were originally developed for electric vehicle applications and use a sodium-conducting beta alumina ceramic as electrolyte and liquid sodium as anode. The positive electrode is $NiCl_2$ in the charged state and Ni in the discharged state, which is impregnated with a Na+ conductive salt ($NaAlCl_4$) offering a diffusion channel between separator and cathode. The specific energy of the conventional tubular $NaNiCl_2$ battery is 95-120 Wh/kg (Yang et al. 2011). In practical applications, it faces the same issues of the NaS battery – cost, high temperature, and safety (Hueso, Armand, and Rojo 2013). Therefore, this battery type is not considered viable for the studied use case.

2.1.4 Flow batteries

Flow Batteries (Fig. 2d), or more formally named redox flow batteries (RFB), are a kind of electrochemical cell where the chemical energy is provided by two electrolyte reservoirs and separated by a membrane (Alotto, Guarnieri, and Moro 2014). The electrochemical processes are realized by means of a reversible redox reaction between the two liquid electrolyte reservoirs. A distinguished advantage of the technology is that the power and energy can be separated since the power is a function of the surface area of the electrodes while the energy capacity is a function of the electrolyte volume (amount of liquid electrolyte) (Alotto, Guarnieri, and Moro 2014). There are many kinds of redox pairs, such as vanadium redox (VRB), zinc-polyiodide (Zn/I), zinc bromine (Zn/Br), polysulfide bromide (PS/B) and cerium zinc (Ce/Zn) (Noack et al. 2015). Organic redox flow batteries are emerging as promising to overcome notable commercialization hurdles faced by inorganic redox flow batteries, but their cycle life and energy density need improvement (Brushett, Vaughey, and Jansen 2012). Flexible energy and power sizing, full discharge ability, safety (non-flammable electrolytes), and no harmful emissions are the advantages, making it a good option for large-scale energy storage for fixed marine energy applications. The drawbacks of the technology lie in low energy density, equipment complexity (pump system) and cost. These lead to limited applicability for the studied use case are not evaluated further.

2.1.5 Metal-air batteries

Metal-Air electrochemical batteries use pure electropositive metal as anode material and external ambient air as the cathode, typically with aqueous or aprotic solutions as electrolyte, to generate electricity. The metal anode includes one of the alkali metals (Li, Na, K), Mg, Al, or transition metals (Fe, Zn) (Fig. 2e); the choice of electrolytes depends on the nature of the anode. An open porous structure is needed for the cathode to support electron exchange and supply oxygen continuity (Li and Lu 2017). The biggest advantage of metal-air batteries is its high theoretical energy density with low cost, which is higher than that of lithium-ion batteries. However, metal-air batteries also face serious barriers, such as low specific energy (i.e., <150 Wh/kg), low efficiency, and short service life (Li and Dai 2014). Though potentially promising with further development, these are not considered for this study.

2.1.6 Lithium-ion batteries

Lithium ion batteries (LIBs) (Fig. 2f) have been widely used in portable electronics, electric vehicles, and large-scale grid energy storage. Compared to other rechargeable battery technologies, LIBs are lighter, smaller and longer lasting. Moreover, the high efficiency, low memory-effect and low self-discharge rate of LIB technology make it a promising option for more and new applications. In principle, during electrochemical reaction processes, lithium ions work as the charge carriers and transfer back and forth between the cathode and anode host structures, realizing the energy storage and release. LIBs can deliver an exceptional cycle life of over a thousand cycles (Hu et al. 2016). However, the operating conditions such as temperature and power output (C rate) have critical impacts on service life. Another barrier for LIB application is the high cost, particularly at large scales. However, the high energy density and cycle life may offset the high capital cost for long deployments (Zhou et al. 2013). This is particularly true for marine applications, where frequent replacement, installation and maintenance are costly.

Despite advantages of high energy density and long cycle life, LIB technology still faces technical challenges when working at extreme scenarios like low/high temperatures and fast charging. This is due to the materials' chemical and electrochemical stability. Particularly, in a marine environment, the LIBs need to potentially withstand the challenges of limited service opportunity, high charge/discharge rates, extreme temperature, pressure, and ocean salinity. We will briefly review existing commercial LIB formulations in the below sections. Since graphite is widely used as the anode material in most LIB technologies, we will focus on pros and cons of various cathodes and their applicability for marine & PBE applications.

2.1.6.1 Layered cathode materials

The layered transition metal oxides (LiMO2, M=Mn, Ni, and Co, Fig. 3a) are the most-used cathode materials in commercial LIBs. $LiCoO_2$, the first-generation layered cathode with extremely high operating cell voltage of 4 V and high electric and Li-ion conductivities, offers the highest power density among all the layered cathodes (Mizushima et al. 1980). However, due to the band overlap between $Co^{3+/4+}$ and O^{2-}: 2p band as shown in Fig. 3b, when Li utilization rate is larger than 50% during the delithiation process, crystal oxygen will be released and causes material failure (Chebiam et al. 2001). This limits specific energy of $LiCoO_2$ to 140 mAh/g with only 50% of Li utilization. High operating temperature makes the oxygen release even easier, causing fast cell failure and safety issues.

The other important layered oxide cathode is $LiNi_{1-x-y}MnxCo_yO_2$ (NMC), which is built by

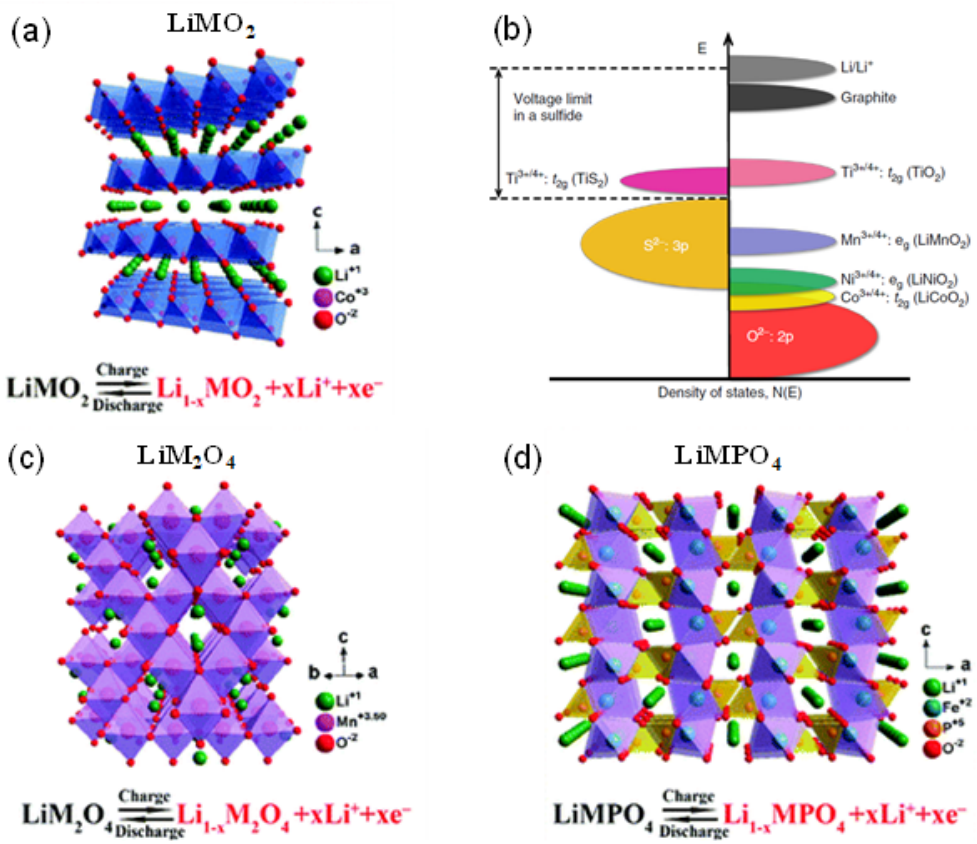

Figure 3. Crystal structures of various cathodes: a) layered $LiMO_2$; c) spinel LiM_2O_4; d) olivine $LiMPO_4$ (Chen et al. 2016); b) Positions of the redox energies relative to the top of the anion: p bands (Manthiram 2020).

substituting Co of the $LiCoO_2$ with Mn and Ni. In NMC cathodes, the valence shell of Ni, Co and Mn are 2+/3+, 3+ and 4+, respectively, and larger specific capacity can be obtained at higher Ni content (Fig. 4) (Noh et al. 2013). However, high Ni content also causes issues of cycle instability, thermal instability and air sensitivity. Moreover, High-Ni cathode materials show serious microcrack generation, which increases side reactions between material particles and electrolyte (Ryu et al. 2018). Hence, to achieve high cycling stability, the Ni content has to be controlled appropriately, depending on the application requirement. For example, NMC333 has promising cycling stability with a reversible capacity of about 160 mAh/g (J. Li et al. 2017), which makes it a good candidate for our analyzed use case application. To improve cell cycle life, particularly at elevated temperature, approaches of cation doping or surface coating (e.g., $LiNi_{1-x-y}Co_xAl_yO_2$ (NCA/NCR)) are usually employed to enhance the material's interfacial and bulk stability (Zhu and Chen 2019). NMC and NCA are two of the chemistries evaluated in the experimental study.

2.1.6.2 Polyanion materials

LIBs utilizing polyanion oxides ($LiMPO_4$, M=Fe, Co, Ni, and Mn) were first reported by Padhi et al. in 1997 (Padhi, Nanjundaswamy, and Goodenough 1997). One of the common commercialized polyanion cathodes is $LiFePO_4$ (LFP) which has relatively high specific capacity

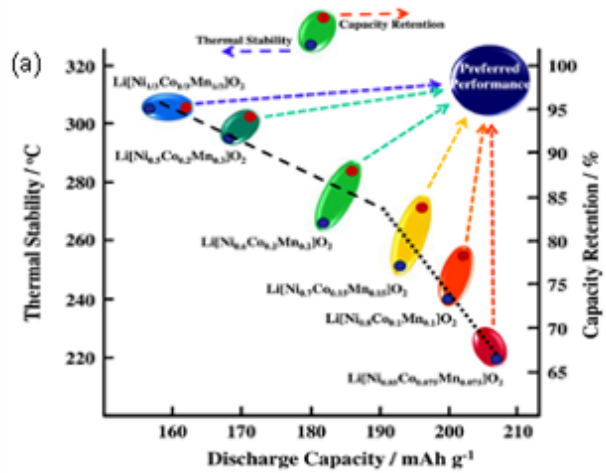

Figure 4. Correlation of discharge capacity with capacity retention and thermal stability (Noh et al. 2013)

of 160 mAh/g (Fig. 3d). This material has significant advantages of low cost, low toxicity, long cycle life, and high safety (Whittingham 2004). Two challenges exist with LFP for high power applications due to the unique crystal structure. First, in LFP structure, the FeO_6 octahedra shares edges with two LiO_6 octahedra and one PO_4 tetrahedra, resulting in low electronic conductivity (Yuan et al. 2011). Second, Li-ion diffusion in LFP is through a 1D diffusion channel along the b-axis direction as shown in Fig. 3d, which is low in diffusivity and easily affected by the Li/Fe mixing (Fig. 5a) (Malik et al. 2010). To overcome the low ionic and electronic conductivity issues, approaches have been adopted in material design: reducing particle size or directional crystal growth (short b direction) (Bi et al. 2013), conductive layer coating, and element doping. Nanosized particles can effectively reduce the diffusion length for Li-ions, improving rate capability. Carbon coating is an effective way to improve material electronic conductivity from 10^{-9} S/cm to 10^{-2} S/cm (Zaghib et al. 2008). Element doping also helps to improve electronic conductivity and thermal stability (Dahn et al. 1994). LFP cells are the third chemistry evaluated in our study.

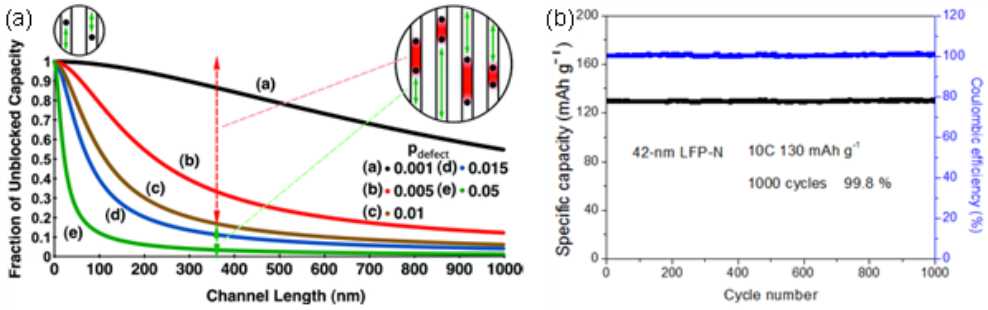

Figure 5. a) The relationship between unblocked capacity and channel length in LFP with different defect concentration (Malik et al. 2010); b) Cycle performance of LFP at 10 C (Duan et al. 2017)

3.0 Methods

Core methodology for the study is split between simulation and experimentation. Each is described below.

3.1 Simulation of the use case

Much of the inspiration for our work investigating energy storage systems suitable for marine energy coupled with ocean observing platforms stems from the operation of NDBC coastal weather buoys at high latitudes. The system's rechargeable LIB pack (Panasonic 18650 NCA/NCR type) is contained in an insulated housing, charged with solar panels, and augmented by a primary (non-rechargeable) battery bank during periods of low solar irradiance. A heater is used to maintain the pack's temperature at 10°C under high state of charge (SOC) conditions, and lower as stored energy decreases (L. LeBlanc, personal communication, May 2020). Temperature regulation is most critical in winter months when the ability to recharge is limited. We hypothesized that wave energy may be a good candidate to augment the existing power system given its complementary seasonality to solar (i.e., strong in winter, low in summer), and may eliminate the need for the secondary battery bank.

A model of NDBC buoy 46081 at Western Prince William Sound in Alaska was implemented in MATLAB-Simulink to determine performance of the system's existing solar array and alternative wind and wave energy sources and compare feasibility for supporting its payload. Though not the focus of this work, wind energy potential was analyzed due to its existing use on similar ocean observing platforms. The particular location was selected as the buoy there has several years worth of wave motion, wind speed, and temperature data to support modeling and is in a location known to have battery and other failures, making it a strong candidate for wave energy integration. The modeled power generation systems were a 1 m diameter heaving point absorber wave energy converter (WEC) with a power rating of 10 kW, a 0.50 m diameter wind turbine with a power rating of 200 W, and a 0.22 m^2 solar array as used on SCOOP buoys.

Methods for estimating the output of representative solar, wind, and wave devices are described in detail in A. E. Copping et al. 2020. The system model used energy input from estimated wave and wind output based on direct measurements at the site and solar irradiance data from the nearby Shelikof Strait on an hourly basis. The model implemented a 10.8 V 140 Ah LIB module from the Simulink library fed through a LIB charging circuit capable of delivering up to 0.25 C charge rate from this input. The 7 kg battery had a specific heat of 950 J/kg/K, 5 Kelvin m^2/W insulation and 0.243 m^2 of surface area and a built-in heater capable of heating from energy input or battery power depending on SOC. The system controlled charging and temperature regulation using a state machine to control system loads based on temperature, power input and SOC. Model process flow and state machine logic are depicted in Fig. 6. The state machine determines which loads are active under a cascade of SOC conditions. For example, State 0 represents a full battery with all buoy systems active. As SOC decreases, subsystems are deactivated until the only remaining load is the buoy processor. One year of typical buoy operation (2017) with multiple energy sources was simulated to capture seasonal trends.

3.2 Experimental evaluation of LIB chemistries

Simulation results and published literature emphasize the outsized impact cell temperature has on the charging and performance of LIBs. We designed and executed an experimental

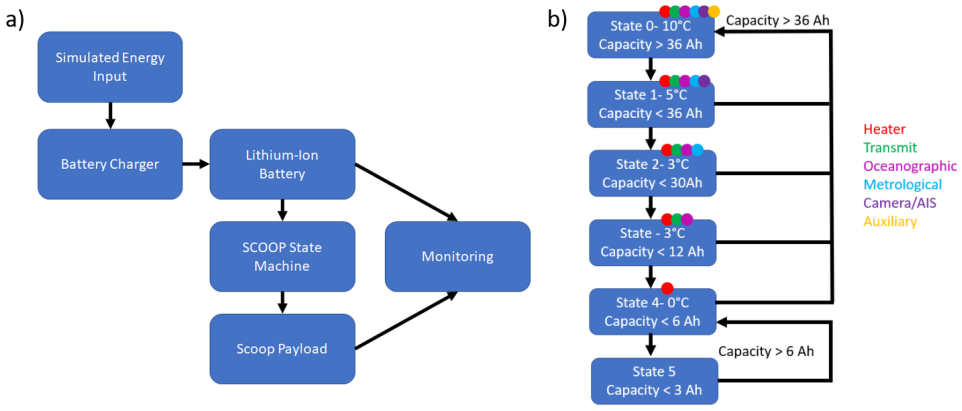

Figure 6. a) SCOOP system simulation layout; b) State machine logic

campaign to evaluate relative performance of three common commercially-available cathode formulations: NMC, NCA, and LFP. Battery performance testing is a systematic process of monitored charge and discharge cycling. For this work, we employed a purpose-built testing system comprised of a Landt CT3001D battery tester with auxiliary voltage monitoring system AT2016A. The Landt tester is comprised of a battery string charge and discharge module with the ability to charge to defined voltages and currents in a sequence of programmed steps, including loops to run through a protocol repeatedly. Accuracy of control is to within mA and mV ranges. The AT2016A voltage monitoring system has the ability to monitor up to 16 additional voltage channels with mV accuracy.

Typical implementations of battery chemistry performance testing evaluate small cells (i.e., units of low practical capacity) for ease of post-processing materials analysis. However, for this work, we are concerned with the performance of battery packs (i.e., strings of larger cells with high capacity) under relevant environmental conditions. To achieve this, strings of three 18650-type cells for each formulation were tested to better understand holistic performance and reliability. Thermistors TEWA TT0P-10KC3-T105-1500 were affixed to the batteries which were placed into 3-unit strings in commercial 18650 battery holders. The full circuit diagram including connection details is shown in Fig. 7.

Strings were situated inside a housing within a 7.6 L double-walled steel flammables storage cabinet (Condor Model 491M60). Vent ports on either side of the cabinet were opened to route cables connecting strings to the testing unit and to vent to the external environment through pliable metal tubing to mitigate potential thermal events. The cabinet was mounted within a structural frame braced on the rim of a 1 m diameter fiberglass tank and sealed with a silicone caulking agent. For testing, the tank was filled with seawater until the lower portion of the cabinet was submerged to ensure the apparatus was thermally-coupled to its environment. The tank was situated in PNNL's Arctic laboratory (Fig. 8), capable of independently controlling water and air temperature. For the duration of the experiment, water temperature setpoint was -3°C – conditions under which seawater freezes and representative of the studied use case in winter months.

Each string was tested utilizing the same protocol (sequence of C rates, where a rate of 1 C is the current draw of the battery delivering its rated capacity over 1 hour), though different combinations of charge and discharge conditions owning to different capacities for each chemistry. After reaching the desired temperature, two formation cycles were applied at

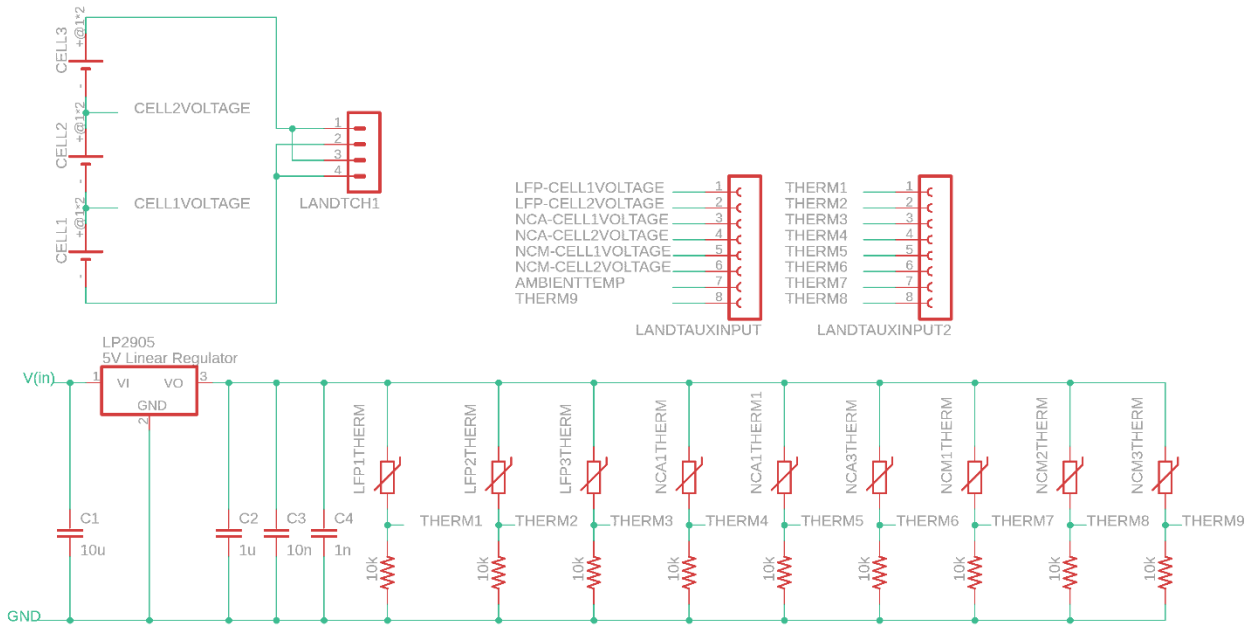

Figure 7. Experimental setup wiring diagram with thermistor arrangement

relatively slow 0.1 C rate in a constant current charge (CCC) to activate the battery with constant current discharge (CCD) cycles in between. Then the strings were charged at 0.5 C with a constant voltage float charge (CVC) and discharged at 2 C for the extended cycling. One capacity check cycle (i.e., 0.1 C for charge/discharge), was performed for every twenty cycles. For example, 2 C discharge of LFP corresponds to a current of 2.2 A, while for NCA and NCM the corresponding currents of 2 C are 4.6 A and 4.8 A, respectively due to the difference of cell capacity (Fig. 9). Charge and discharge voltages were selected to imitate commercial battery under/over-voltage safety cutoffs. These charge/discharge conditions terminated when the specified criteria were met, allowing the protocol to continue to the next step.

Battery strings were cycled through the described protocol while current, voltage, and temperature were measured for both individual cells and strings. These measurements were used to determine battery capacity over time (i.e., number of cycles), ultimately representing battery life. The average battery can withstand 500-1,000 full charge/discharge cycles depending on chemistry and other factors. Our testing is designed to stress the batteries under harsh conditions similar to our use case. Most LIBs have a 0°C minimum temperature rating for charging with no guarantee of cell function below that threshold, and many failure modes for LIBs involve a thermal event. Additional testing was conducted to more closely emulate the charge and discharge cycling of the buoy power system use case using a single string of three LFP cells. The protocol is set up to bulk charge the LIB up to high capacity at C/2 but not conduct float and conditioning charge steps. Following charging, the cells are set to discharge 25% at 1 C for 600 s. This protocol (Fig. 10) was designed to stress the LIB in its working capacity range and reveal possible degradation mechanisms by increasing the number of times bulk charging was applied to a cold cell.

Raw binary data from the data logger was exported into a .csv using software provided by Landt and subsequently parsed into a Matlab data structure for analysis and plotting. A smoothing (rolling average) filter was applied to thermistor data for visualization purposes to make trends more apparent. Coulombic efficiency was calculated for each complete charge/discharge cycle as the ratio of discharge capacity to charge capacity.

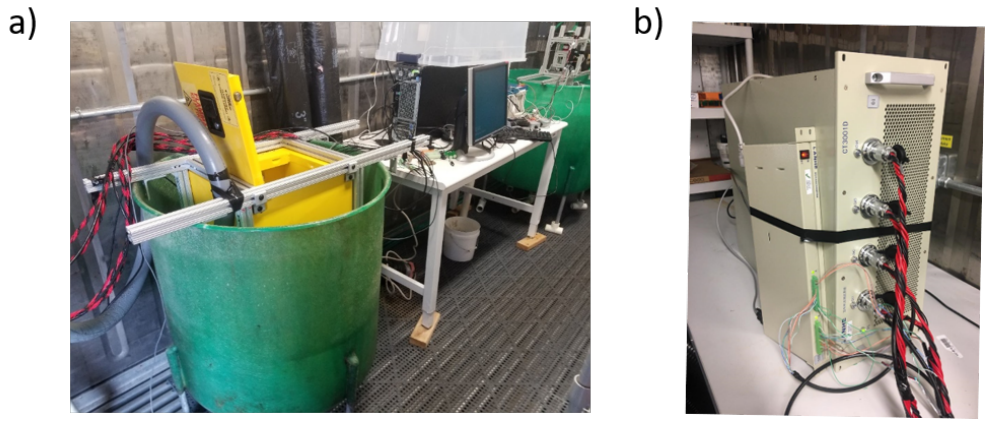

Figure 8. a) Testing apparatus situated in the PNNL Arctic Simulation lab; b) Battery testing hardware

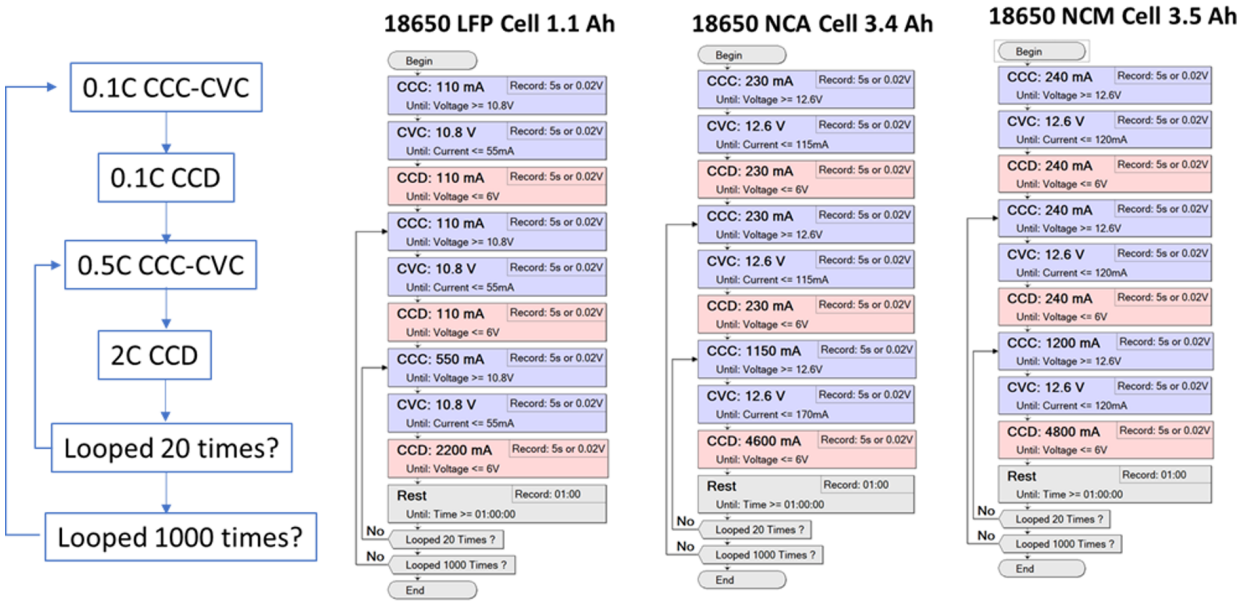

Figure 9. Main testing protocol and program steps for the three evaluated chemistries

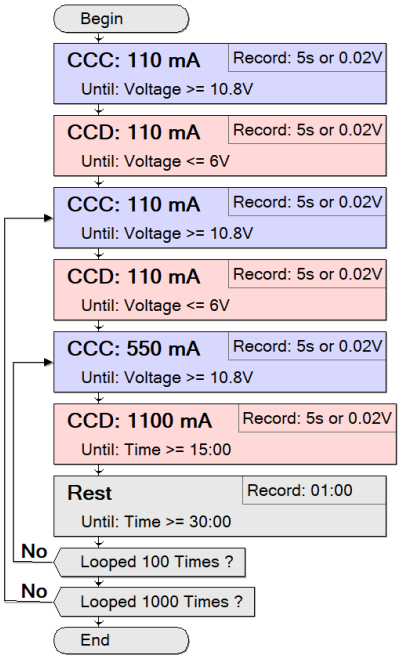

Figure 10. Testing protocol for rapid charge of a separate LFP string

4.0 Results

4.1 Simulation results

The multi-resource and battery storage system was simulated over a full year. As expected, solar availability is highest in summer months with relatively steady daily output that tapers in winter months to virtually no energy harvested. The output of solar is inversely correlated to the availability of wave and wind energy by season. Wind and wave power output are driven by storms with the majority of the energy harvested during intense bursts in winter and surrounding months, as shown in Fig. 11. Single storm events and the power generated by the wind and wave systems are capable of charging the entire battery under the simulation conditions, as depicted in Fig. 12. Conversely, the buoy's existing solar array would take approximately 3 months to bring the battery to full SOC under the same conditions (Fig. 13).

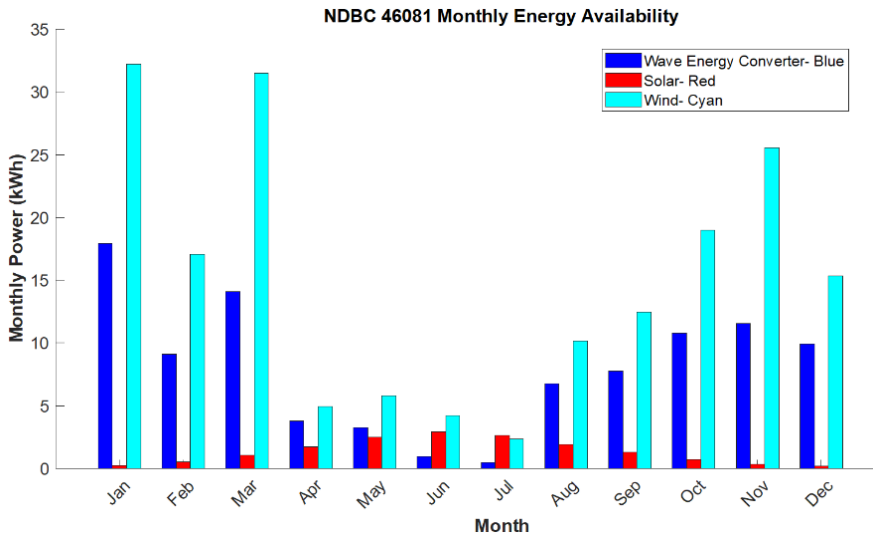

Figure 11. Simulated monthly energy harvested at NDBC station 46081

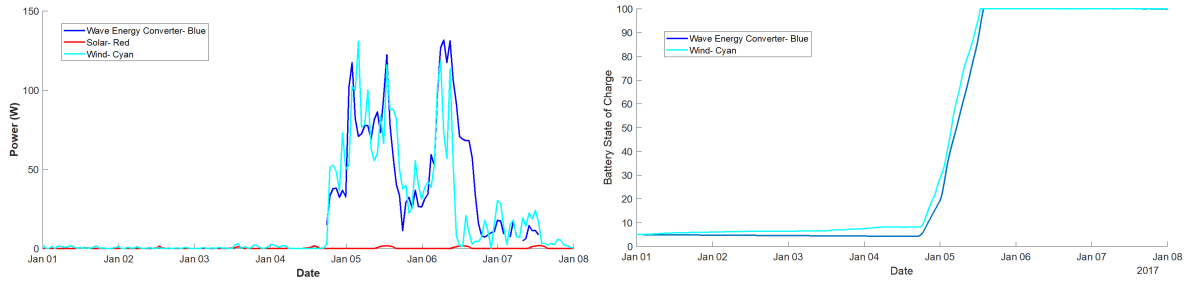

Figure 12. Energy available by resource (left) and charging off WEC and wind energy (right) from one storm event

Differences in the intensity and periodicity between solar and wind/wave have implications for charging the buoy's LIBs. Battery specifications state that charging must be conducted above 0°C as the cells will be irreversibly damaged if charged at low temperatures (Power Electronics Online 2008). Power from waves and wind may be more efficient for charging LIBs specifically because the bulk of the power is delivered in short bursts. In the case of solar, the

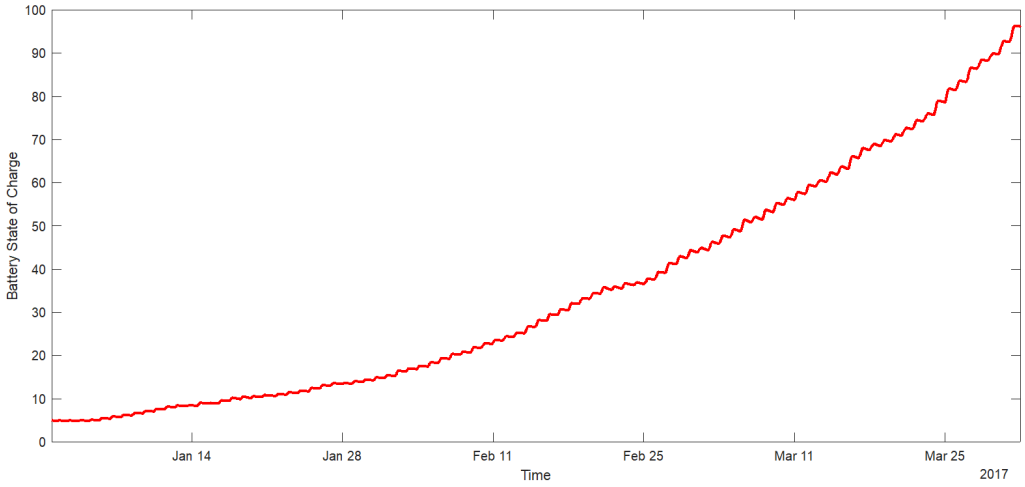

Figure 13. Solar input to the modeled SCOOP buoy's state of charge

batteries must be heated every day before charging commences, and in winter months much power is spent doing so. A significant portion of the harvested energy is thus utilized to maintain the battery bank. The profile of charging from wave and wind energy is very different as a typical winter storm gradually builds over the course of several hours, then spikes, leading to a surge in available charging energy. As LIBs can be charged quickly once they have reached a sufficient temperature, the majority of power delivered during storm events is used directly for charging instead of as heat during a daily heating cycle.

4.2 Room temperature tests and temperature control

Each battery string was cycled through 10 runs of a baseline protocol at room temperature to verify performance under standard operating conditions. Baseline performance for each chemistry is established in terms of rate capability and cycling stability. The cell strings were cycled with the following protocol: 1st cycle charged/discharged both at 0.1 C; the subsequent cycles were charged at 0.5 C and discharged at 1 C. For the LFP string, at 0.1 C charge/discharge, the cell string delivers a reversible capacity of 1.16 Ah with a mid-voltage of 9.5 V (Fig. 14a). When it is charged at 0.5 C and then discharged at 2 C, the reversible discharge capacity is identical to that at low 0.1 C rate. The only difference was observed on the charge/discharge plateaus, where higher charging voltage and lower discharging curves are observed at elevated C rates. This is a normal phenomenon for batteries and ascribed to the increase of electrochemical polarization (variation from the theoretical voltage) at elevated current densities. Upon cycling, the LFP string shows very stable cycling stability without seeing any decay of either capacity or voltage plateau. Very similar behaviors were observed for both NCA and NCM cell strings. As shown in Fig. 14c, d, e and f, NCA and NCM strings exhibit almost identical discharge capacities at the both low and high C rates, as well as stable cycling. These results indicate that at room temperature each chemistry has acceptable rate capability and cycling stability.

Temperature throughout the main protocol experimental period fluctuated within a roughly 1°C hysteresis band, resulting in an average temperature of -2.4°C, compared to the setpoint of -3°C. Lab temperature is plotted over time and presented as Fig. 15.

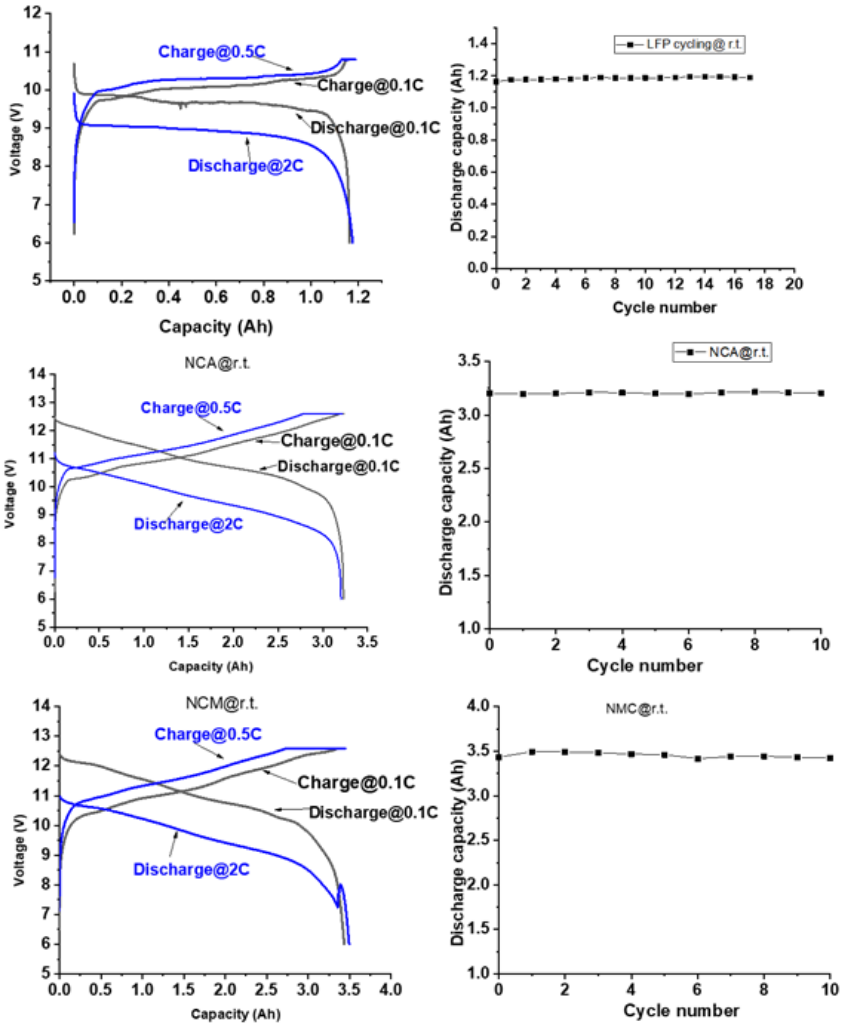

Figure 14. Charge/discharge curves and capacity retention of LFP, NCA, and NCM at room temperature and various C rate to benchmark the cell performance at normal conditions

4.3 Main protocol results

Results for each chemistry are presented, reporting typical charge and discharge behavior at low temperature, discharge capacity and voltage, capacity retention, and evolution of Coulombic efficiency and mid-cycle discharge voltage over cycle count.

Fig. 16 shows electrochemical performance of the LFP string tested at low temperature. Fig. 16a compares string charge/discharge voltages at low and high C rates. At 0.1 C, the string exhibits a low polarization, featuring low mid-charge voltage (10.0 V) and high mid-discharge voltage (9.5 V). When the cycling was switched to 0.5 C charge and 2 C discharge, polarization grows significantly with observations of both increase of charging voltage and decrease of discharging voltage. One interesting observation is that when operated at high currents (i.e., 2 C rate for discharge), the cell string has much higher reversible capacity (about 1.05 Ah) if compared with that (about 0.8 Ah) at low current (0.1 C). This is due to the heat generation and propagation at high current densities, which will be discussed in the following sections. The

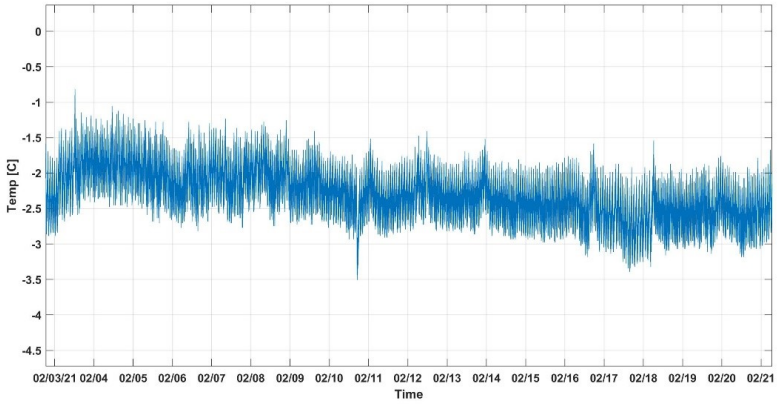

Figure 15. Lab temperature throughout the experimental period

LFP string shows exceptional cycling stability at low temperature. As shown in Fig. 16c, the string has a capacity retention of 102% after 200 cycles, meaning the LFP cells did not exhibit capacity decay during the test. To the contrary, there was a measurable increase in capacity.

Fig. 17 shows electrochemical performance of the NCA string at low temperature. Fig. 17a compares the string's charge/discharge voltage at low and high rates. Similar to the observations of LFP string, during 0.1 C charge/charge processes, the string exhibits lower polarization while exhibiting a lower discharge capacity. With increase of current density, the reversible capacity increases while the corresponding discharge voltage decreases. This indicates important effects of heat generation at high C rate, which helps to warm up the cells and thus enhances capacity release. For cycling stability, the NCA string shows inferior performance in terms of both discharge capacity and voltage compared to the LFP string. As shown in Fig. 17c, the discharge capacity degrades after repeated cycling commences. After 200 cycles, the capacity retention is 72%. Accompanying the capacity fading, cell voltage also shows a gradual decay trend, indicating slow active material degradation or gradual growth of solid electrolyte interface (SEI) on the graphite anode under these low temperature conditions.

Fig. 18 shows electrochemical performance of the NCM string tested at low temperature. Compared to LFP and NCA strings, the NCM string performs in sharp contrast in terms of capacity retention and polarization. These observations were confirmed in repeated tests (i.e., multiple iterations with NCM strings). Observations are summarized as follows: First, at low (0.1 C) and high (2 C) C rates, the NCM string has almost identical capacities (Fig. 18a). This likely suggests that NCM's baseline performance is not as sensitive to temperature as LFP and NCA. Second, the NCA has much worse cycling stability compared with both NCA and LFP. As shown in Fig. 18d, the capacity starts to decay from the 20th cycle and is completely degraded by the 46th cycle. The results of capacity check cycles at 0.1 C indicate the string still has the high capacity, comparable to the original value but loses the ability to deliver current at the 2 C discharge rate. This is also confirmed by the charge/discharge curves. As shown in Figs. 18b and c, the cell discharge voltage steadily decreased and easily reached the cutoff voltage at the very beginning of the 47th cycle discharge, leading to the very limited discharge capacity.

It was found that temperature and its evolution play a critical role in cell performance when cycled at low temperature. Accordingly, temperature evolution of each cell of the string was monitored during the cycling. Figs. 19a and c compare the voltage-capacity profiles of each LFP cell. Voltage variations exist among the three cells of the string and are ascribed to the temperature difference. Figs. 19b and d exhibit the temperature change of each cell during charging and discharging, respectively. Cell charging at 0.5 C generates heat and warms up

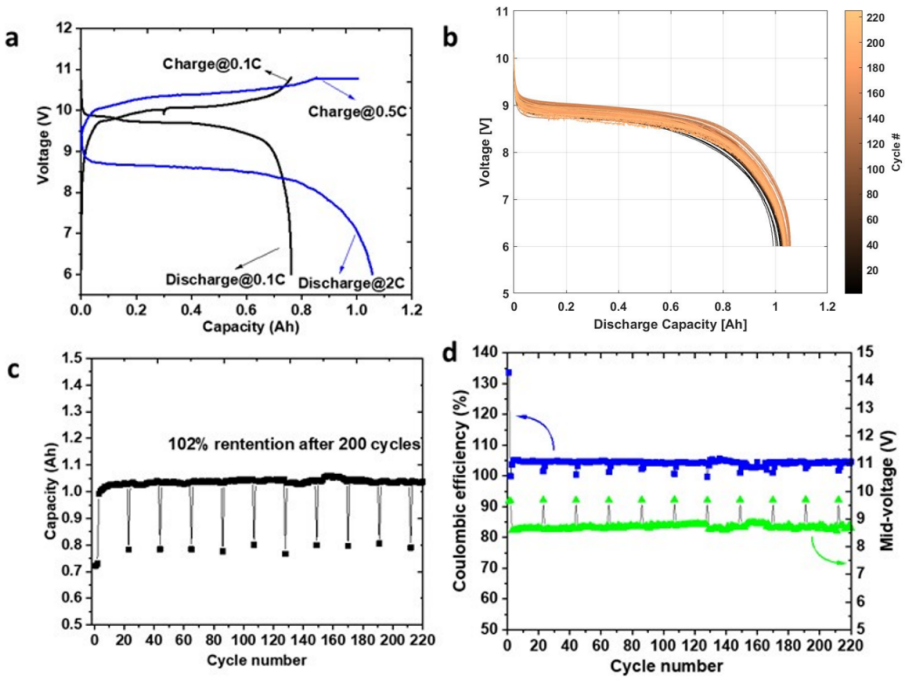

Figure 16. a) Typical charge/discharge curves of LFP at different C rates and low temperature; b) Evolution of discharge curves during 220 cycles; c) Capacity retention with cycling; d) Evolution of Coulombic efficiency and mid-cycle discharge voltage

the cells, resulting in a 3 degree increase in temperature, while the cell temperature recovers during the constant current charge (CCC) process. This suggests the applied current density plays a dominant role in cell heating. This speculation is supported by the temperature response when cells are discharged at the higher 2 C rate. As shown in Fig. 19d, driven by the high current, more heat was generated in each cell and the corresponding temperature increases by 15-20 degrees. Such a quick increase of temperature plays a critical role in reducing cell polarization at low temperature thus improves the discharge capacity. It is clear the cells with higher temperatures within the string show higher discharge voltage. An additional observation is that cell #2 of the string usually has a higher temperature and increasing rate. It may be due to the string configuration, where cell #2 is always positioned between cell #1 and #3. This means in addition to cell chemistry and current density, heat propagation/accumulation is also an important factor, which should be carefully considered when designing the cell string, pack, or module. Similar temperature evolution trends were observed in NCA and NCM strings. One major difference is that NCA and NCM have even higher temperature increase (20-30 degree) compared to LFP. Two possible reasons account for this difference: 1) at given C rates, higher currents were applied in NCA and NCM strings, and 2) poor rate capability of NCA and NCM chemistry. Compared to NCA and NCM, the LFP cells are coated with conductive carbon layers during the materials manufacturing process granting much higher electronic conductivity, making it more suitable for high power applications.

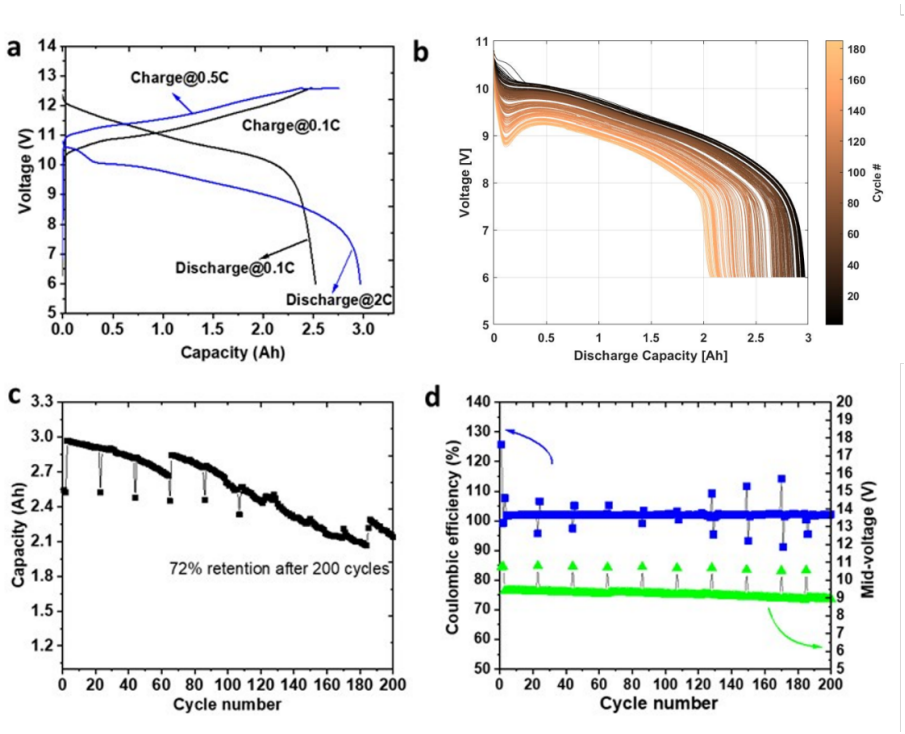

Figure 17. a) Typical charge/discharge curves of NCA at different C rates and low temperature; b) Evolution of discharge curves during 220 cycles; c) Capacity retention with cycling; d) Evolution of Coulombic efficiency and mid-cycle discharge voltage

4.4 Rapid cycling protocol results

The test protocol for the rapidly-cycled LFP string was run for over seven hundred cycles, reporting peak voltage with cell capacity and working range charge/discharge characteristics. No significant changes in cell capacities were observed over seven hundred charge discharge cycles held at an average temperature of -2.4 C. The cells were not given a float charge to balance string capacity, however cell capacities remain above 97% of their initial value and show no evidence of degradation or failure modes as seen in NCA and NCM during rapid discharge. These conditions exposed the LFP string to discharge current densities twice that of other formulations.

The charge characteristics of the rapid-cycling LFP testing, as seen in Fig. 20, are to charge from approximately 75% capacity instead of charging from a low voltage cutoff (i.e., depleted capacity) as in the more traditional main protocol testing. Measurements during cycling demonstrate a consistent profile with slight variation.

While discharging the LFP string (Fig. 20), more fluctuation in voltage with capacity is observed than while charging. While the initial string voltage was on the lower end of the curve for all the cycles, it gradually improved over the course of 500 cycles before reverting to approximately the average of all cycles. Though minor, this trend indicates there may be additional variables impacting performance.

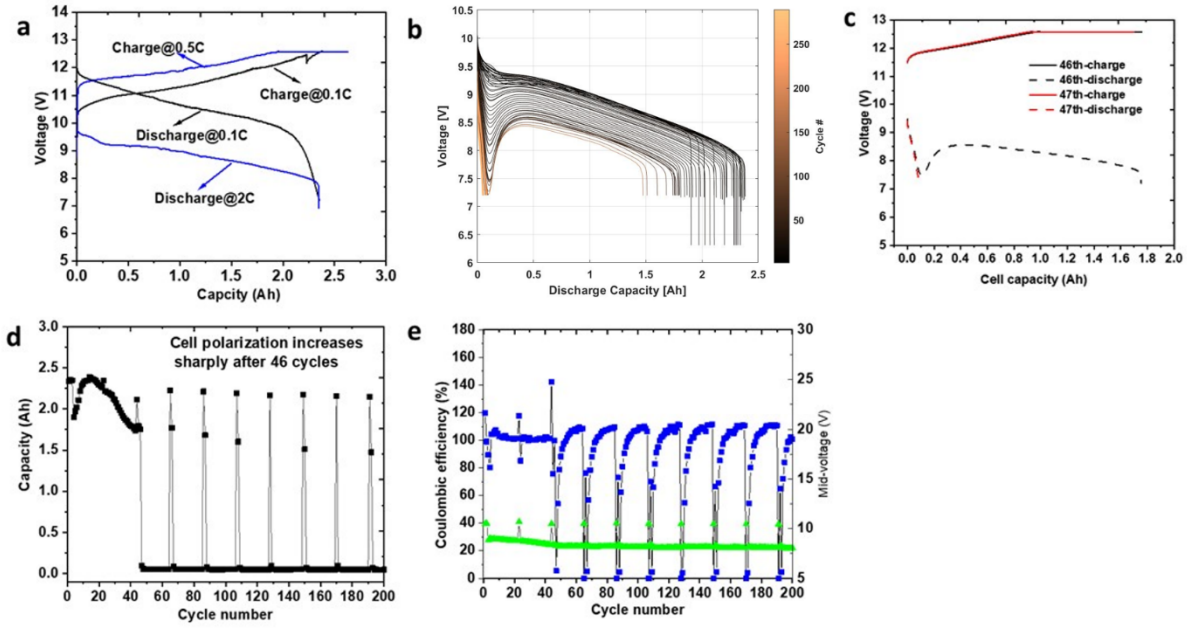

Figure 18. a) Typical charge/discharge curves of NCM at different C rates and low temperature; b) Evolution of discharge curves during 220 cycles; c) Capacity retention with cycling; d) Evolution of Coulombic efficiency and mid-cycle discharge voltage

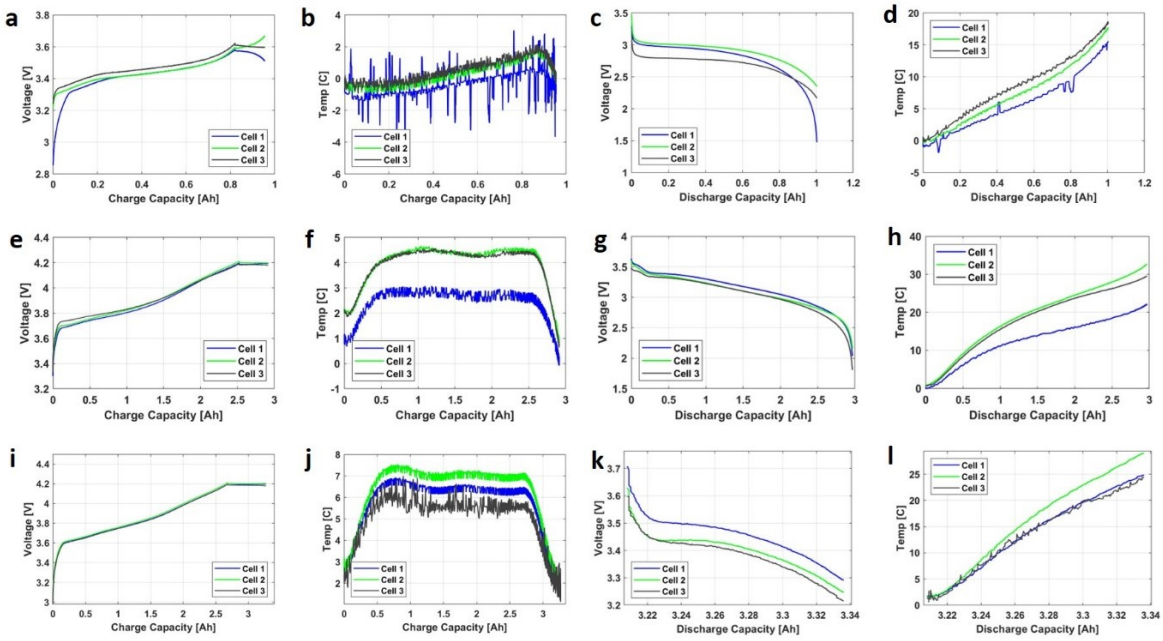

Figure 19. Charge/discharge profiles of each cell of string and corresponding temperature evolution (4th cycle of each string): a:d) LFP string; e:h), NCA string; i:l), NCM string

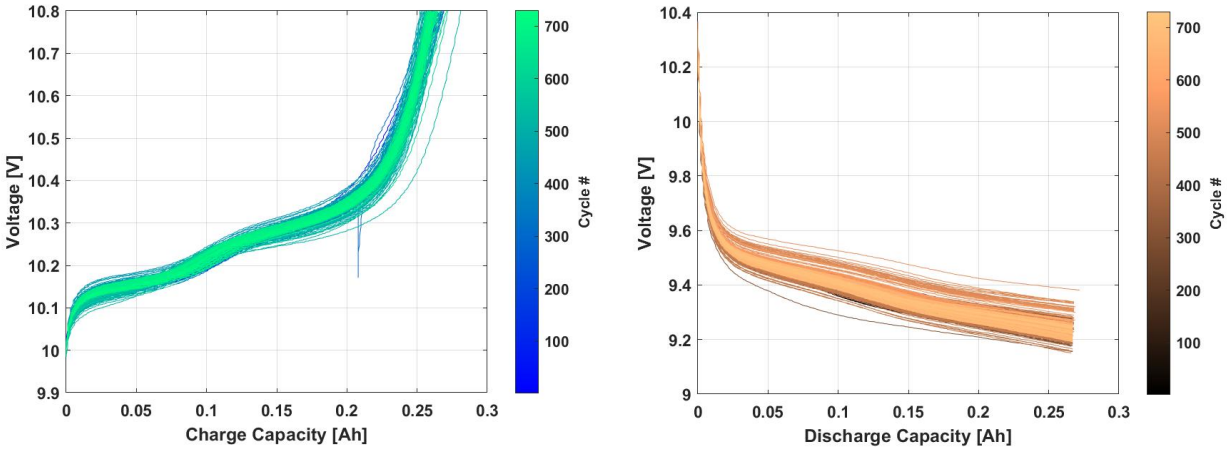

Figure 20. Charge (left) and discharge (right) of LFP cells discharged 25% over 700 cycles

5.0 Discussion

Our simulation results show there may be benefit to the high-intensity periodicity of marine energy for battery function and health. Energy storage for cold locations is essential to their missions and the ability to charge only over a threshold temperature results in significant portions of available solar energy being used to heat the cells instead of going into a bulk charge. With a significantly higher resource intensity and, at least for the studied location, a tendency to produce significantly higher amounts of power than would be possible with solar during storm events enables rapid charging - the bulk of which is spent on replenishing capacity and not on heat. Given that simulations show that a modestly sized WEC (1 m diameter) should be capable of fully recharging a battery during storm events, integration of wave energy may enable additional functionality, such as higher power sensors, more on-board computing, and more frequent data transmissions.

Comparison of cell chemistries at room temperature and temperatures associated with high-latitude marine operation strongly suggests that temperature is a critical factor in determining cell performance, especially cell lifespan. Despite the nominal performance of all the chemistries at room temperature, at an average temperature of -2.4°C, only the LFP string functioned to deliver normal capacity and cycling stability. For NCA and NCM, quick capacity decay was observed with cycling. More detailed study is needed to understand the cell failure mechanism under low temperature and string test conditions. The published mode for damage to LIBs at low temperature is usually related to lithium plating on the graphite anode as a result of worse Li diffusivity in graphite or across the graphite solid electrolyte interface (SEI). Deposited Li metal is extremely reactive and thus easy reacts with liquid electrolyte. This results in both lithium inventory loss and formation of interfacial resistive layers on the graphite surfaces, leading to cell capacity decay and voltage increase. Cell damage caused by SEI formation is irreversible and progressive and can cause long term damage leading to a catastrophic thermal event or loss of battery function. For NCA and NCM chemistries utilized in low-temperature applications, new designs of materials, electrolyte or cells are needed to overcome this poor performance. The other important observation from the study is that high C rate charge or discharge actually has positive effects on cell capacity for LFP chemistries. The effect was evident at low temperature charge/discharge cycles regardless of temperatures and remained true through increased heat generation and accumulation with higher current. In addition, the cell configuration within strings, string configuration within packs, and pack enclosure composition and arrangement are likely to impact heat propagation and will have an effect on cell performance variation. Heat generation and management require further study and should be correlated to cell chemistry and cell operating conditions like temperature and current density (C rate). This comes with a caveat; capacity loss is partially recoverable with increases in temperature. NCM cells in particular highlight this activity when cell voltage drops precipitously early in the bulk charging stage, then recovers dramatically as cell temperature increases. The overall capacity is still reduced and any high load applications become unfeasible as useful cell capacity becomes low over the course of repeated cycling. These chemistries may remain useful for low temperature discharge applications, though progressive cell polarization is likely to eventually reduce capacity to unusable levels regardless of temperature if charged at less than manufacturers' specified temperatures.

The stability of LFP batteries at low temperatures is promising for applications in a variety of harsh environments. While the published specification for charging temperature for LFP cells is the same as any other battery (over 0°C), our results suggest they do not suffer damage to their anode or polarization effects as other lithium chemistries do. Design of insulating or climate-controlled battery enclosures may be less demanding or altogether unnecessary, reducing system complexity and/or cost. Given many PBE applications will be designed to have

long service lives with limited opportunities for maintenance and the high cost of recovery, LFP may be the most suitable choice for future implementations. However, improved performance for practical applications may come at the expense of higher volume required for energy storage; LFP cells have around one third the baseline capacity of the more common NCA and NCM formulations.

Significant degradation leading to failure of NCM strings was observed after around 50 cycles, while a steady decay towards failure was observed for NCA strings over 200 cycles. LFP strings showed no degradation through the same 200 cycles of the main testing protocol, and were additionally subjected to conditions most likely to lead to cell polarization from temperature effects over 700 cycles. While it can not be ruled out that LFP cells will not eventually fail from temperature related effects, 700 cycles approach the several thousand cycles used in industrial battery testing. It was assumed (as is the case for our intended use case) that the battery housing is thermally coupled to seawater, which is at a significantly higher temperature than other relevant cold-climate environments. Other specific environments of interest are terrestrial Arctic applications (e.g., Alaska at -35°C) where energy storage of any battery chemistry requires heating for efficient performance. Non-terrestrial applications for polar orbiting satellites and lunar installations (-170°C) and the Martian surface (-60°C) are of interest to a wide variety of modern developers and as LIBs are encapsulated in hermetically sealed pouches and have minimal off-gassing, these cells should perform in space much as they do on Earth. Future research avenues leading from this study may consider test-to-failure cycling and colder environmental conditions.

6.0 Conclusions

Ocean observing platforms are a high value-proposition potential early-adopter market for marine energy, and rely on energy storage systems that require special accommodation in cold climates at sea. A number of options exist for battery energy storage, with lead-acid and lithium-ion batteries being the most common and appropriate for this application. Lithium-based options offer superior energy density, though are known to be sensitive to temperature extremes at both the low and high ends, resulting in diminished capacity or catastrophic runaway. A model simulating an NDBC SCOOP buoy in a high-latitude coastal Alaska location and estimated solar, wind, and wave energy output showed how the higher resource intensity of the latter two and power generated during storm events may be sufficient to completely charge the system's battery bank. Charging in this manner is a more efficient method, as it does not require frequent re-heating of the battery bank prior to bulk charging.

Systematic battery performance testing of three commercially-available lithium-ion battery formulations (NMC, NCA, and LFP) was conducted in environmental conditions emulating a platform operating in freezing seawater. A main testing protocol of cyclic charging and discharging over 200 iterations triggered degradation of useful capacity for the NMC string after about 50 cycles, and showed a trending decline in useful capacity for the NCA string over all cycles. The LFP string suffered no discernible degradation over the duration of testing. Subsequent rapid cycling testing of the LFP string yielded similar results (i.e., no performance change) over 700 cycles. LFP batteries are recommended for further study and use for cold-climate at sea implementations because of their strong performance in this experimental campaign.

References

Alotto, Piergiorgio, Massimo Guarnieri, and Federico Moro. 2014. "Redox flow batteries for the storage of renewable energy: A review." *Renewable and sustainable energy reviews* 29:325–335.

Bi, Zhiying, Xudong Zhang, Wen He, Dandan Min, and Wanshuo Zhang. 2013. "Recent advances in LiFePO 4 nanoparticles with different morphology for high-performance lithium-ion batteries." *RSC Advances* 3 (43): 19744–19751.

Brushett, Fikile R, John T Vaughey, and Andrew N Jansen. 2012. "An all-organic non-aqueous lithium-ion redox flow battery." *Advanced Energy Materials* 2 (11): 1390–1396.

Cavagnaro, R. J., A. E. Copping, R. Green, D. Greene, S. Jenne, D. Rose, and D. Overhus. 2020. "Powering the Blue Economy: Progress Exploring Marine Renewable Energy Integration With Ocean Observations." *Marine Technology Society Journal* 54 (6): 114–125. ISSN: 0025-3324. https://doi.org/doi:10.4031/MTSJ.54.6.11. https://www.ingentaconnect.com/content/mts/mtsj/2020/00000054/00000006/art00012.

Cavagnaro, R. J., C. Matthews, D. Hume, R. Raye, A. Copping, and S. Jenne. 2020. "Enabling Marine Energy Integration for OceanObserving: Functional Requirements." In *OCEANS 2020 MTS/IEEE GLOBAL,* 1–7.

Chebiam, RV, Arunachala Mada Kannan, F Prado, and A Manthiram. 2001. "Comparison of the chemical stability of the high energy density cathodes of lithium-ion batteries." *Electrochemistry communications* 3 (11): 624–627.

Chen, Renjie, Taolin Zhao, Xiaoxiao Zhang, Li Li, and Feng Wu. 2016. "Advanced cathode materials for lithium-ion batteries using nanoarchitectonics." *Nanoscale horizons* 1 (6): 423–444.

Chew, Gilbert, Dennis G Pelaccio, and Diane Johnson. 2002. "Study of power system upgrades for NDBC buoys." In *OCEANS'02 MTS/IEEE,* 1:388–395. IEEE.

Copping, Andrea, Al LiVecchi, Heather Spence, Alicia Gorton, Scott Jenne, Robert Preus, Gary Gill, Robi Robichaud, and Simon Gore. 2018. "Maritime Renewable Energy Markets: Power From the Sea." *Marine Technology Society Journal* 52 (5): 99–109. https://doi.org/10.4031/MTSJ.52.5.3.

Copping, Andrea E., Rebecca Green, Robert J. Cavagnaro, Dale S. Jenne, David Greene, Jayson J. Martinez, and Yang Yang. 2020. "Powering the Blue Economy - Ocean Observing Use Cases Report" (February). https://doi.org/10.2172/1700536. https://www.osti.gov/biblio/1700536.

Dahn, JR, EW Fuller, M Obrovac, and U Von Sacken. 1994. "Thermal stability of LixCoO2, LixNiO2 and λ-MnO2 and consequences for the safety of Li-ion cells." *Solid State Ionics* 69 (3-4): 265–270.

Divya, KC, and Jacob Østergaard. 2009. "Battery energy storage technology for power systems—An overview." *Electric power systems research* 79 (4): 511–520.

Duan, Yandong, Bingkai Zhang, Jiaxin Zheng, Jiangtao Hu, Jianguo Wen, Dean J Miller, Pengfei Yan, Tongchao Liu, Hua Guo, Wen Li, et al. 2017. "Excess Li-ion storage on reconstructed surfaces of nanocrystals to boost battery performance." *Nano letters* 17 (10): 6018–6026.

Green, R., A. Copping, R. J. Cavagnaro, D. Rose, D. Overhus, and D. Jenne. 2019. "Enabling Power at Sea: Opportunities for Expanded Ocean Observations through Marine Renewable Energy Integration." In *OCEANS 2019 MTS/IEEE SEATTLE,* 1–7. https://doi.org/10.23919/OCEANS40490.2019.8962706.

Hadjipaschalis, Ioannis, Andreas Poullikkas, and Venizelos Efthimiou. 2009. "Overview of current and future energy storage technologies for electric power applications." *Renewable and sustainable energy reviews* 13 (6-7): 1513–1522.

Hu, Jiangtao, Yi Jiang, Suihan Cui, Yandong Duan, Tongchao Liu, Hua Guo, Lingpiao Lin, Yuan Lin, Jiaxin Zheng, Khalil Amine, et al. 2016. "3D-printed cathodes of LiMn1- xFexPO4 nanocrystals achieve both ultrahigh rate and high capacity for advanced lithium-ion battery." *Advanced Energy Materials* 6 (18): 1600856.

Hueso, Karina B, Michel Armand, and Teófilo Rojo. 2013. "High temperature sodium batteries: status, challenges and future trends." *Energy & Environmental Science* 6 (3): 734–749.

Joslin, J, E Cotter, P Murphy, P Gibbs, R Cavagnaro, C Crisp, Andy R Stewart, Brian Polagye, Patrick S Cross, Even Hjetland, et al. 2019. "The wave-powered adaptable monitoring package: hardware design, installation, and deployment." In *Proceedings of the 13th European Wave and Tidal Energy Conference, Naples, Italy,* 1–6.

Li, Guosheng, Xiaochuan Lu, Jin Y Kim, Kerry D Meinhardt, Hee Jung Chang, Nathan L Canfield, and Vincent L Sprenkle. 2016. "Advanced intermediate temperature sodium–nickel chloride batteries with ultra-high energy density." *Nature communications* 7 (1): 1–6.

Li, Jing, Andrew R Cameron, Hongyang Li, Stephen Glazier, Deijun Xiong, M Chatzidakis, Jenn Allen, GA Botton, and JR Dahn. 2017. "Comparison of single crystal and polycrystalline LiNi0. 5Mn0. 3Co0. 2O2 positive electrode materials for high voltage Li-ion cells." *Journal of The Electrochemical Society* 164 (7): A1534.

Li, Yanguang, and Hongjie Dai. 2014. "Recent advances in zinc–air batteries." *Chemical Society Reviews* 43 (15): 5257–5275.

Li, Yanguang, and Jun Lu. 2017. "Metal–air batteries: will they be the future electrochemical energy storage device of choice?" *ACS Energy Letters* 2 (6): 1370–1377.

LiVecchi, A., A. Copping, D. Jenne, A. Gorton, A. Preus, G. Gill, R. Robichaud, et al. 2019. "Powering the Blue Economy; Exploring Opportunities for Marine Renewable Energy in Maritime Markets." *U.S. Department of Energy, Office of Energy Efficiency and Renewable Energy. Washington, D.C.,* 207. https://www.energy.gov/eere/water/downloads/powering-blue-economy-report.

Malik, Rahul, Damian Burch, Martin Bazant, and Gerbrand Ceder. 2010. "Particle size dependence of the ionic diffusivity." *Nano letters* 10 (10): 4123–4127.

Manthiram, Arumugam. 2020. "A reflection on lithium-ion battery cathode chemistry." *Nature communications* 11 (1): 1–9.

Mizushima, K, PC Jones, PJ Wiseman, and John B Goodenough. 1980. “LixCoO2 (0< x<-1): A new cathode material for batteries of high energy density.” *Materials Research Bulletin* 15 (6): 783–789.

Noack, Jens, Nataliya Roznyatovskaya, Tatjana Herr, and Peter Fischer. 2015. “The chemistry of redox-flow batteries.” *Angewandte Chemie International Edition* 54 (34): 9776–9809.

Noh, Hyung-Joo, Sungjune Youn, Chong Seung Yoon, and Yang-Kook Sun. 2013. “Comparison of the structural and electrochemical properties of layered Li [NixCoyMnz] O2 (x= 1/3, 0.5, 0.6, 0.7, 0.8 and 0.85) cathode material for lithium-ion batteries.” *Journal of power sources* 233:121–130.

Ouyang, Dongxu, Yaping He, Jingwen Weng, Jiahao Liu, Mingyi Chen, and Jian Wang. 2019. “Influence of low temperature conditions on lithium-ion batteries and the application of an insulation material.” *RSC advances* 9 (16): 9053–9066.

Padhi, Akshaya K, Kirakodu S Nanjundaswamy, and John B Goodenough. 1997. “Phospho-olivines as positive-electrode materials for rechargeable lithium batteries.” *Journal of the electrochemical society* 144 (4): 1188.

Parker, Carl D. 2001. “Lead–acid battery energy-storage systems for electricity supply networks.” *Journal of Power Sources* 100 (1-2): 18–28.

Power Electronics Online. 2008. *Proper Care Extends Li-Ion Battery Life | Power Electronics.* https://www.powerelectronics.com/markets/mobile/article/21859861/proper-care-extends-liion-battery-life. (Accessed on 06/18/2021).

Ryu, Hoon-Hee, Kang-Joon Park, Chong S Yoon, and Yang-Kook Sun. 2018. “Capacity fading of Ni-rich Li [Ni x Co y Mn1–x–y] O2 (0.6≤ x≤ 0.95) cathodes for high-energy-density lithium-ion batteries: bulk or surface degradation?” *Chemistry of materials* 30 (3): 1155–1163.

Sudworth, JL. 1984. “The sodium/sulphur battery.” *Journal of power sources* 11 (1-2): 143–154.

Whittingham, M Stanley. 2004. “Lithium batteries and cathode materials.” *Chemical reviews* 104 (10): 4271–4302.

Yang, Zhenguo, Jianlu Zhang, Michael CW Kintner-Meyer, Xiaochuan Lu, Daiwon Choi, John P Lemmon, and Jun Liu. 2011. “Electrochemical energy storage for green grid.” *Chemical reviews* 111 (5): 3577–3613.

Yuan, Li-Xia, Zhao-Hui Wang, Wu-Xing Zhang, Xian-Luo Hu, Ji-Tao Chen, Yun-Hui Huang, and John B Goodenough. 2011. “Development and challenges of LiFePO 4 cathode material for lithium-ion batteries.” *Energy & Environmental Science* 4 (2): 269–284.

Zaghib, K, A Mauger, F Gendron, and CM Julien. 2008. “Surface effects on the physical and electrochemical properties of thin LiFePO4 particles.” *Chemistry of Materials* 20 (2): 462–469.

Zhou, Zhibin, Mohamed Benbouzid, Jean Frédéric Charpentier, Franck Scuiller, and Tianhao Tang. 2012. “Energy storage technologies for smoothing power fluctuations in marine current turbines.” In *2012 IEEE International Symposium on Industrial Electronics,* 1425–1430. Ieee.

Zhou, Zhibin, Mohamed Benbouzid, Jean Frédéric Charpentier, Franck Scuiller, and Tianhao Tang. 2013. “A review of energy storage technologies for marine current energy systems.” *Renewable and Sustainable Energy Reviews* 18:390–400.

Zhu, Jian, and Guoying Chen. 2019. “Single-crystal based studies for correlating the properties and high-voltage performance of Li [Ni x Mn y Co 1- x- y] O 2 cathodes.” *Journal of Materials Chemistry A* 7 (10): 5463–5474.

Zubi, Ghassan, Rodolfo Dufo-LÃ³pez, Monica Carvalho, and Guzay Pasaoglu. 2018. “The lithium-ion battery: State of the art and future perspectives.” *Renewable and Sustainable Energy Reviews* 89:292–308. ISSN: 1364-0321. https://doi.org/https://doi.org/10.1016/j.rser.2018.03.002. https://www.sciencedirect.com/science/article/pii/S1364032118300728.

Pacific Northwest National Laboratory

902 Battelle Boulevard
P.O. Box 999
Richland, WA 99352
1-888-375-PNNL (7675)

www.pnnl.gov